2004

An Empirical Study of Frost Accumulation Effects on Louvered-Fin, Microchannel Heat Exchangers

Yan Ping Xia
University of Illinois at Urbana-Champaign

Predrag S. Hrnjak
University of Illinois at Urbana-Champaign

Anthony M. Jacobi
University of Illinois at Urbana-Champaign

AN EMPIRICAL STUDY OF FROST ACCUMULATION EFFECTS ON LOUVERED-FIN, MICROCHANNEL HEAT EXCHANGERS

Y. Xia[1], P. S. Hrnjak[2] and A. M. Jacobi[3]

Department of Mechanical and Industrial Engineering, University of Illinois
Urbana, IL, USA
Fax: (217) 244-6534, Phone: (217) 333-2328, E-mail: xia@uiuc.edu[1]
Fax: (217) 244-6534, Phone (217) 649-3163, E-mail: pega@uiuc.edu[2]
Fax: (217) 244-6534, Phone (217) 649-3162, E-mail: a-jacobi@uiuc.edu[3]

ABSTRACT

The use of folded-louvered-fin, microchannel heat exchangers in refrigeration and heat pump applications, where normal operating conditions give rise to frost accumulation on the airside heat transfer surface, is experimentally studied. Heat transfer and pressure drop data are presented for heat exchangers with different fin geometries. The visualization of frost growth via a 0.5mm fiberscope indicates that the bridging of louver gap by frost contributes to a decrease in airside heat transfer coefficient as the frosting process evolves. The bridging of the louver gap implies that the airside flow pattern changes from a louver-directed to a duct-directed flow, with a deleterious impact on heat transfer. The impacts of frost growth on heat transfer and thermal-hydraulic performance for different fin geometries are compared in terms of *f* and *j* factors.

1. INTRODUCTION

Folded-louvered-fin, microchannel heat exchangers are usually constructed by brazing folded (sometimes called serpentine) fins to extruded microchannel tubes. This type of heat exchanger is finding wider application as performance, compactness and cost concerns continue to drive heat exchanger design. In order to use folded-fin microchannel heat exchangers in heat-pump or refrigeration systems where frosting occurs, the effect of frost accumulation on their performance must be characterized.

Over the past several decades, a lot of research has been done on frost properties and growth in simple geometries. O'Neal and Tree (1985) provided a review of frost formation in simple geometries, and more recent work on frost formation on a cold flat plate or parallel horizontal plates includes that of Östin and Anderson (1991), Tao *et al*. (1993), Sherif *et al*. (1993), Lee *et al*. (1997). However, few reports are available for the more complex geometries of finned tube heat exchangers, and very little has been published to address frost formation on louvered-folded-fin, flat-tube heat exchangers. Kondepudi and O'Neal (1987) provided a review of frost growth on extended surface heat exchanger performance, and Kondepudi and O'Neal (1989) conducted research on the louvered finned heat exchangers. Unfortunately, because almost no performance data are available, there are almost no design guidelines for using microchannel heat exchangers under frosting conditions. Moreover, although the general effects of frost growth–causing decrease in the overall heat transfer coefficient and increase in the pressure drop across the heat exchanger–are well known, they have not been explored in quantified details.

In this paper, the airside performance characteristics of louvered-fin microchannel heat exchangers under frosting conditions will be evaluated, with attention on the effects of fin geometry. Heat transfer and pressure drop data will be presented for a variation of louvered-fin designs. The visualization of frost growth via a 0.5mm fiberscope will be shown to explain the effect of the bridging of louver gap by frost on the airside heat transfer coefficient. The impacts of frost growth on heat transfer and thermal-hydraulic performance for different fin geometries are compared in terms of *f* and *j* factors.

2. EXPERIMENTAL METHOD

2.1 Experimental Apparatus and Test Procedure

The experimental facility (Carlson *et al*., 2001) used to test microchannel heat exchangers under frosting conditions is shown in Figure 1. An open wind tunnel was placed inside an environmental chamber. The heat exchanger is placed immediately in front of the wind tunnel, hung on an electronic balance to measure the accumulated frost mass. Flexible plastic film was used to connect the heat exchanger to the tunnel, allowing the heat exchanger to move freely in the vertical direction for proper frost mass measurement. The heat exchanger was circuited in a pure cross-flow configuration. The airflow was horizontal and the tubes were vertical. A precooler was included in the chamber to precool the chamber to the desired temperature.

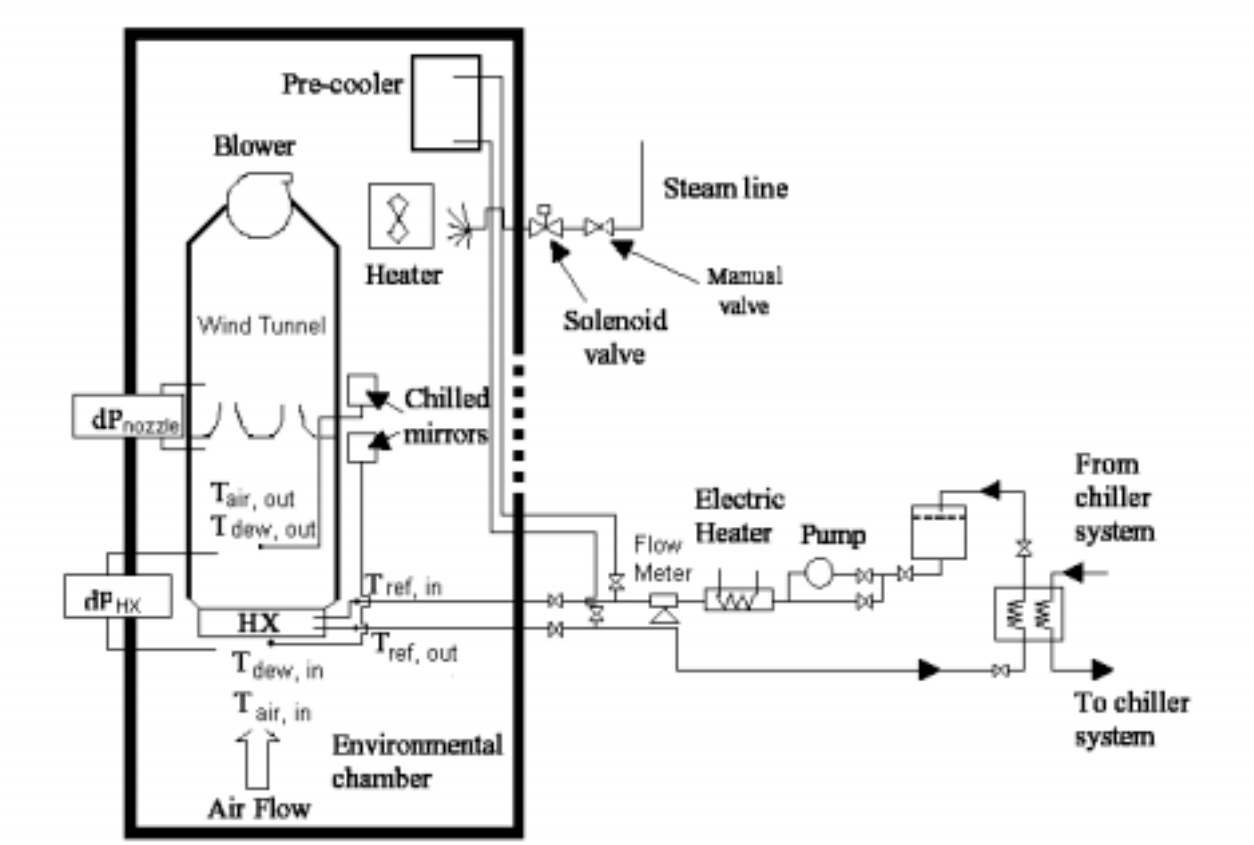

Figure 1: Facility schematic

Airflow was provided using a variable speed blower, and was measured using two nozzles. Pressure taps, placed on both sides of the nozzles, were connected to a pressure transducer so that the pressure drop across the nozzles could be measured and used to determine the air mass flow rate. The air temperature is controlled using a PID controller to regulate the power supplied to the heater located in the chamber according to a thermocouple sensor placed at the inlet of the heat exchanger. Humidification was provided by a steam line, and was controlled using a dew-point chilled-mirror sensor and PID controller. The air humidity data were obtained by two chilled-mirror sensors (including the one for humidity control). Air temperatures were measured using two thermocouple grids at the inlet and exit of the heat exchanger. The airside pressure drop across the heat exchanger was measured with another pressure transducer connected to the static pressure taps in the test section.

Ethyl alcohol supplied by a gear pump was used in the experimental loop. The alcohol flow, as the coolant for the test section, was cooled by a chiller system, and its temperature was regulated using an electrical heater and a PID controller. The coolant temperatures were measured using immersion thermocouples at the inlet and exit of the heat exchanger. A mass flow meter was used to measure the mass flow rate of the coolant.

The data acquisition system sampled instruments throughout the tests and recorded data to a text file for subsequent analysis. Readings were obtained every 10 seconds, and the averaged values were collected every minute. Still images and videos of frost growth were obtained with a CCD camera and a 0.5mm fiberscope.

At the initiation of an experiment, coolant was sent to the precooler alone until the chamber was cooled to the desired temperature. After achieving the desired chamber temperature, the coolant was diverted to the heat exchanger and performance data collected. The experiments were conducted at constant air-inlet temperature, refrigerant-inlet temperature, air-inlet humidity, refrigerant mass flow rate, and blower frequency. The test conditions are given in Table 1.

Table 1: Test conditions

Air Inlet Temperature [˚C]	Refrigerant Average Temperature [˚C]	Relative Humidity	Initial Face Velocity [m/s]
-1	-9	80%	1.0

2.2 Data Reduction Method

The ultimate objective of this data reduction is to obtain the *j* and *f* factors for the air-side surface. Basic data analysis includes determining the capacity of the heat exchanger, which is calculated from both the coolant side and the air side, using

$$Q_{ref} = \dot{m}_{ref}\left(Cp_{ref,out}T_{ref,out} - Cp_{ref,in}T_{ref,in}\right), \quad (1)$$

and

$$Q_{air} = \left(\dot{m}_{air,in}Cp_{air,in}T_{air,in} - \dot{m}_{air,out}Cp_{air,out}T_{air,out}\right) + \dot{m}_{frost}h_{sg}, \quad (2)$$

The heat balance, which is defined in below, was within 10%:

$$HB = \frac{2\times\left|Q_{ref} - Q_{air}\right|}{Q_{ref} + Q_{air}}. \quad (3)$$

In order to isolate the air-side convective heat transfer coefficient, h_o, the overall thermal resistance is considered. Neglecting the conduction resistance of the tube wall, the overall thermal resistance can be considered as composed of air-side convection and a coolant-side convection, i.e.,

$$\frac{1}{UA} = \frac{1}{\eta_o h_o A_o} + \frac{1}{h_i A_i}. \quad (4)$$

In Equation (4), the overall heat transfer coefficient is obtained from

$$UA = Q_{air,sens} / \Delta T_{lm}, \quad (5)$$

where ΔT_{lm} is the log-mean temperature difference.

With respect to the coolant side, the flow is laminar, and appropriate correlations for Nusselt number recommended by Shah and London (1978) are used according to the shape of the ducts and the flow conditions (hydrodynamically/thermally developing/developed flow). Thus, the coolant-side convective heat transfer coefficient is obtained by

$$h_i = \frac{Nu_i \cdot k_i}{D_i}. \quad (6)$$

On the air side, the overall surface efficiency η_o is obtained using

$$\eta_o = 1 - \frac{A_{fin}}{A_o}(1-\eta), \quad (7)$$

where η, the fin efficiency, accounts for the effect of deposited frost. Under frosting conditions, the frost layer and the fin form a composite medium. Using the effective conductivity of the frost, the problem can be regarded as a heat conduction problem in a two-layer body. Xia and Jacobi (2004) justified the simplification of the problem as

heat conduction in a two-dimensional frost layer composite with a one-dimensional thin fin, and provided an analytical solution to this problem. The one-term approximation to this solution is used in this work, with an error of no more than 3% up to a frost thickness of 0.9 mm, namely:

$$\eta = \frac{\lambda}{h_o L \delta_{frost}} \frac{\sinh\left(\frac{\lambda L}{\delta_{frost}}\right)}{\cosh\left(\frac{\lambda L}{\delta_{frost}}\right)} \left(k_{fin} t + k_{frost} \delta_{frost}\right), \tag{8}$$

where

$$\lambda = \delta_{frost} \sqrt{\frac{h_o}{k_{fin} t + \delta_{frost}\left(k_{fin} h_o t / k_{frost} + k_{frost}\right)}}. \tag{9}$$

In the above two equations, h_o is determined by iteration. Frost conductivity is obtained using the correlation provided by Lee *et al*. (1997),

$$k_{frost} = 0.132 + 3.13\times10^{-4} \rho_{frost,avg} + 1.6\times10^{-7} \rho_{frost,avg}^2 . \tag{10}$$

The averaged frost density is calculated using

$$\rho_{frost,avg} = m_{frost} / (\delta_{frost} A_o) . \tag{11}$$

There are two ways to obtain the frost thickness δ_{frost}. One method uses the frost images captured using the CCD camera (a front view of the heat exchanger) as the one shown in Figure 2.

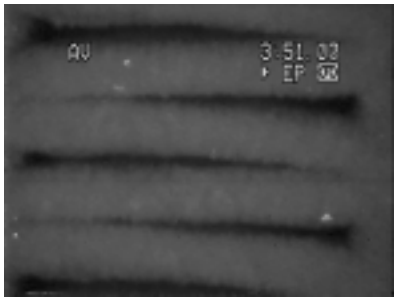

Figure 2: Frost image recorded by focusing a CCD camera on the front view of the heat exchanger

The other method relies on the empirical correlation suggested by Hayashi *et al.* (1977) to get the frost surface density, which is integrated over time as follows:

$$\rho_{frost,s} = 650 \exp(0.277 \cdot T_s) , \tag{12}$$

and

$$\delta_{frost} = \int_0^\tau \dot{m}_{frost} / (A_o \rho_{frost,s}) dt . \tag{13}$$

The frost surface temperature T_s in Equation (12) is obtained from the Chilton Colburn analogy. The log-mean humidity ratio difference is calculated from

$$\Delta\varpi_{lm} = \frac{\dot{m}_{frost} Cp_{air}}{h_o A_o \mathrm{Le}^{-2/3}} , \tag{14}$$

where Le is Lewis number, and the log-mean humidity ratio difference $\Delta\omega_{lm}$ is defined as

$$\Delta\varpi_{lm} = \frac{(\varpi_{in} - \varpi_s) - (\varpi_{out} - \varpi_s)}{\ln\left[(\varpi_{in} - \varpi_s)/(\varpi_{out} - \varpi_s)\right]} . \tag{15}$$

With $\Delta\omega_{lm}$ known, the humidity ratio at the frost surface, ω_s, can be computed. If the air-vapor mixture in the neighborhood of the frost layer is considered as saturated, then ω_s corresponds to the humidity ratio of the air-vapor mixture at the frost surface temperature. Thus, T_s is determined.

The two methods for determining frost thickness on the heat exchanger are from images of the heat exchanger face and from the model described above. The frost thickness as obtained from these methods is compared for one experimental condition in Figure 3. In the first method, the exact frost boundary is difficult to determine, and that might contribute to the discrepancy, especially early in the growth cycle. Moreover, images of the leading edge of the fin might not be representative of the entire heat exchanger. The drawback to the second method is that it ignores the amount of water vapor absorbed in the frost layer; thus, it is expected to over estimate thickness. It must be noted that this method is dependent on the correlations used for density and conductivity, and these properties are generally hard to predict for frost. It can be seen that the error between the two methods is about 20% at a frost thickness of 1mm, while the thickness increase rates are close to each other after the first 10 minutes.

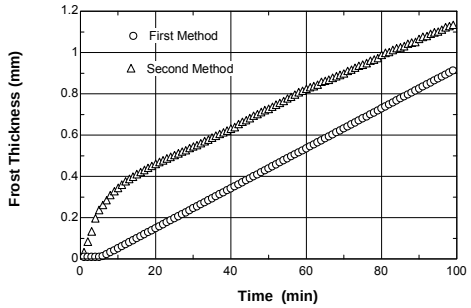

Figure 3: A comparison of the frost thickness obtained with different method

Equations (1)-(15) are closed; i.e., the number of equations equals the number of unknowns, with measured variables taken as known. The data are used with this equation set to iterate to the correct h_o. Next, h_o is used to calculate the Nusselt number, and then the Stanton number and j factor:

$$\mathrm{St} = \frac{\mathrm{Nu}}{\mathrm{Re}\cdot \mathrm{Pr}}, \tag{16}$$

$$j = \mathrm{St}\cdot \mathrm{Pr}^{2/3}, \tag{17}$$

where Pr is Prandtl number. Note that the Reynolds number and Nusselt number in the above equations are all based on the hydraulic diameter, which is adjusted to account for frost deposition on the heat exchanger as time passes. The calculation of f factor is relatively simple as compared to j factor. It is obtained by

$$f = \frac{2\Delta P_{HX}\rho_{avg}}{G^2}\left(\frac{A_c}{A_{tot}}\right) - \left(1+\sigma^2\right)\left(\frac{\rho_{in}}{\rho_{out}} - 1\right)\left(\frac{A_c}{A_{tot}}\right)\left(\frac{\rho_{avg}}{\rho_{in}}\right), \tag{18}$$

where

$$\sigma = \frac{A_c}{A_{frontal}} \tag{19}$$

and again, A_c is adjusted in time to account for the deposition of frost.

3. RESULTS

3.1 Heat Transfer and Pressure Drop

The heat transfer and pressure drop data for three different fin geometries are shown in Figure 4, with the geometries listed in Table 2 and fin structure shown in Figure 5. The overall heat transfer coefficient is normalized with the initial value. The decrease in the overall heat transfer coefficient and increase in the pressure drop can be observed. It is noteworthy that the performance of the third fin type is quite different from the other two. The major difference in the third specimen is that it has a much larger fin length than the other two designs, i.e. a long air flow path. It is shown by Figure 4 that the pressure drop increase rate for this type of fin decreases towards the end of the experiment, which implies a longer operation time before the pressure drop reaches a set value (a typical control variable for de-frosting). However, its overall heat transfer coefficient decreases to only 20% of the initial value.

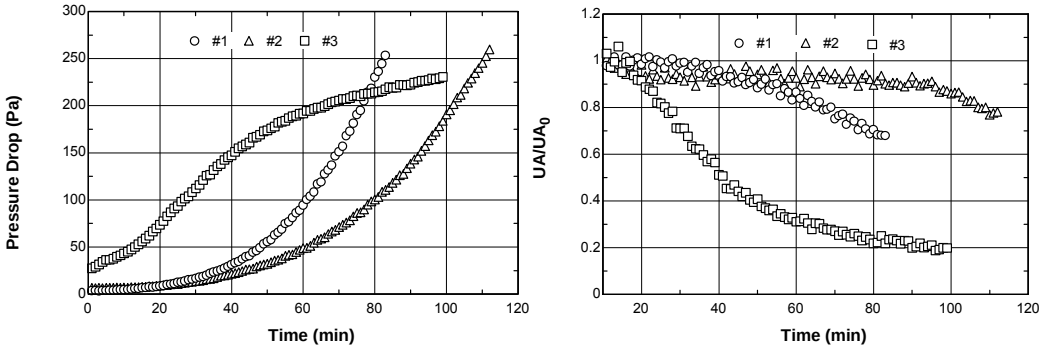

(a) (b)

Fgure 4: Heat Transfer and pressure drop data for different fin geometries

Table 2: Fin geometries

Specimens	#1	#2	#3
Fin density (fpm)	670	472	472
Fin height, H (mm)	8.9	7.3	9.1
Fin length, Lf (mm)	16.5	27.9	77.0
Louver length, Ll (mm)	7.50	5.90	6.25
Louver angle, θ (˚)	23	27	30
Louver pitch, Lp (mm)	1.0	1.4	1.5

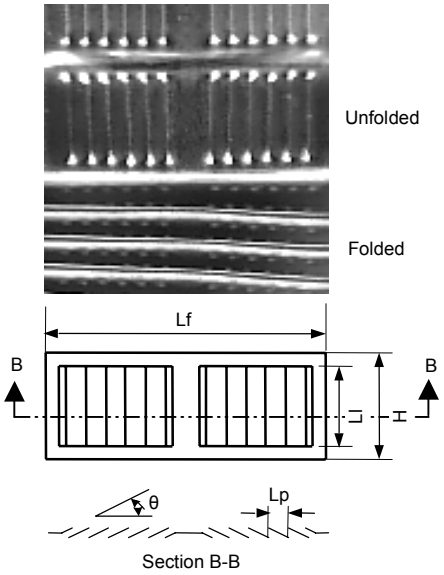

Fgure 5: Structure of the louvered fin

3.2 Air Side Heat Transfer Coefficient

In this research, a fiberscope is used to provide insight into the frost deposition patterns on the fins. The fiberscope is a kind of flexible boroscope, with an outer diameter of 0.5 mm. The fiberscope tip can be inserted into the inter-fin space to record what is happening. The scope was focused on a fixed location within the louver array. The first louver entering the visual field can be clearly seen. Figure 6(a) shows a series of images recorded by the fiberscope. At the 36th minute, the inter-louver gap (A) was blocked by frost. As can be seen from Figure 5(b), the airside heat transfer coefficient begins to drop approximately after the first 30 minutes. The bridging of the louver gap implies that the airside flow pattern changes from louver directed to duct directed, with a deleterious impact on heat transfer. Apparently, inter-louver bridging by frost is responsible for a decrease in airside heat transfer coefficient.

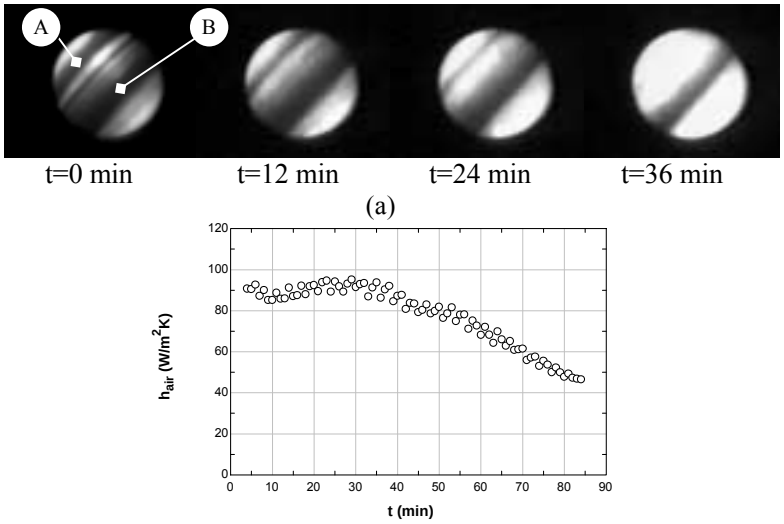

Figure 6: Air-side heat transfer coefficient begins to decrease as soon as the louver gap is blocked by frost: (a) Frost images by a 0.5mm fiberscope, where A and B indicate louver gap and fin gap respectively; (b) Air-side heat transfer coefficient vs. time

3.3 *j* and *f* Factors

The *j* and *f* factors corresponding to the fin geometries listed in Table 2 are provided in Figure 7. The *j* and *f* factors are also normalized with the initial value, and the x-coordinate is the nondimensional frost thickness Γ, which is defined as frost thickness over fin pitch. As frost growths, the normalized *j* factor for all three types of fin decreases, with similar behavior for all the heat exchangers. The effects on *f* factor are complex, and need further investigation.

.

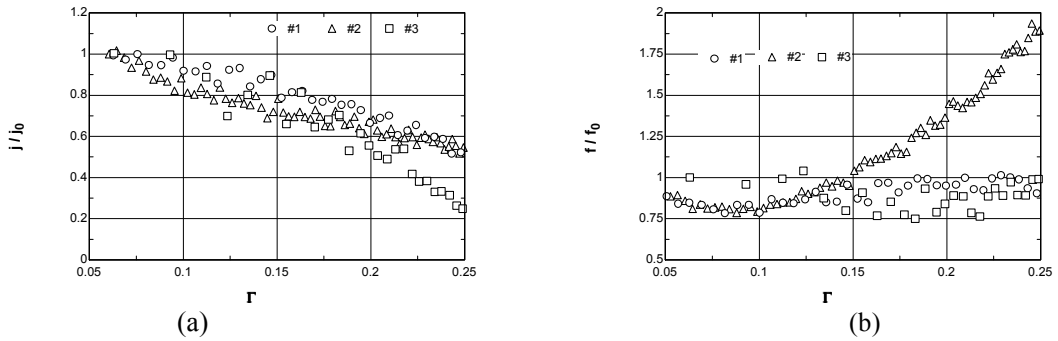

Figure 7: *j* and *f* factors for different fin geometries

6. CONCLUSIONS

The use of folded-louvered-fin, microchannel heat exchangers in refrigeration and heat pump applications is experimentally studied. The experimental facility is described, and the data reduction method is explained. The heat transfer and pressure drop across the heat exchanger data for three different fin geometries are presented, and a decrease in the overall heat transfer coefficient and increase in the pressure drop can be observed as frost grows. The pressure drop increase for fins with a large depth decreases towards the end of an experiment, implying longer operation time before a defrost. The bridging of louver gaps by frost is one major reason for the decrease in airside heat transfer coefficient.

NOMENCLATURE

A	area	(m^2)
Cp	specific heat	($Jkg^{-1}{}^oC^{-1}$)
D	hydraulic diameter	(m)
G	Air flow mass velocity	($kgm^{-2}s^{-1}$)
h	heat transfer coefficient	($Wm^{-2}{}^oC^{-1}$)
h_{sg}	latent heat	(Jkg^{-1})
k	thermal conductivity	($Wm^{-1}{}^oC^{-1}$)
L	half the distance between tubes	(m)
m	mass	(kg)
$\dot{m}$	mass flow/deposit rate	(kg/s)
ΔP_{HX}	pressure drop across heat exchanger	(Pa)
Q	heat transfer	(W)
t	half fin thickness	(m)
T	temperature	(ºC)
UA	overall heat transfer coefficient	(W^oC^{-1})
δ	frost thickness	(m)
Γ	frost thickness over fin pitch	(–)
η	fin efficiency	(–)
λ	a fin efficiency parameter	(–)
ρ	density	(kgm^{-3})
ω	humidity ratio	(kg water/kg dry air)

Subscripts

air	air
avg	average
c	free flow
f in	fin
frontal	frontal
frost	frost
i	refrigerant side
in	inlet
o	air side
out	outlet
ref	refrigerant
s	frost surface
sens	sensible heat
tot	total transfer area

REFERENCES

O'Neal, D. L., Tree, D. R., 1985, Review of frost formation in simple geometries, *ASHRAE Trans*, vol. 91, no. 2: p. 267–281.

Östin, R. and Anderson, S., 1991, Frost growth parameters in a forced air stream, *Int. J. Heat Mass Transf.*, vol. 34, no. 4/5: p. 1009–1017.

Tao, Y.-X., Besant, R. W., Mao, Y., 1993, Characteristics of frost growth on a flat plate during the early growth period, *ASHRAE Trans*, vol. 99: p. 746–753.

Sherif, S. A., Raju, S. P., Padki, M. M., Chan, A. B., 1993, A semi-empirical transient method for modeling frost formation on a flat plate, *Int. J. Refrig.*, vol. 16, no. 5: p. 321–329.

Lee, K. S., Kim, W. S., Lee, T. H., 1997, A one-dimensional model for frost formation on a cold flat surface, *Int. J. Heat Mass Transf.*, vol. 40, no. 18: p. 4359–4365.

Kondepudi, S. N., O'Neal, D. L., 1987, Effects of frost growth on extended surface heat exchanger performance – a review, *ASHRAE Trans*, vol. 93, no. 2: p. 258-274.

Kondepudi, S. N., O'Neal, D. L., 1989, Effect of frost growth on the performance of louvered finned tube heat exchangers, *Int. J. Refrig.*, vol. 12: p. 151–158.

Carlson, D. M., Hrnjak, P. S., Bullard, C. W., 2001, Deposition, Distribution, and Effects of Frost on a Multi-Row Heat Exchanger Performance, ACRC TR-183, University of Illinois, Urbana-Champaign.

Shah, R. K., London, A. L., 1978, *Laminar Flow Forced Convection in Ducts – A Source Book for Compact Heat Exchanger Analytical Data*, Academic Press, New York.

Hayashi Y., Aoki A., Adachi S., 1977, Study of frost properties correlating with frost formation types, *Journal of Heat Transfer*, vol. 99: p. 239–245.

Xia, Y., Jacobi, A. M., accepted January 2004, An exact solution to steady heat conduction in a two-dimensional slab on a one-dimensional fin: application to frosted heat exchangers, *Int. J. Heat Mass Transf.*

ACKNOWLEDGEMENT

We are grateful for financial support from the Air Conditioning and Refrigeration Center (ACRC) at the University of Illinois and the Air-Conditioning and the Air-Conditioning and Refrigeration Technology Institute (ARTI).